ELSEVIER

Chemical Engineering Journal 139 (2008) 84–92

Chemical Engineering Journal

www.elsevier.com/locate/cej

Flow subjected to porous blocks in the cavity: Consideration of block aspect ratio and porosity

S.Z. Shuja, B.S. Yilbas *, S.M.A. Khan

ME Department, KFUPM Box 1913, Dhahrann 31261, Saudi Arabia

Received 8 May 2007; received in revised form 17 July 2007; accepted 18 July 2007

Abstract

Thermal analysis of the flow over porous blocks in the cavity is examined and the effects of the aspect ratio and porosity of the blocks on the flow field and heat transfer rates are predicted numerically. In the simulations, two blocks with three porosities and two aspect ratios are considered. Air is used as the working fluid. The equilibrium-based equations are accommodated in the analysis and the control volume approach is introduced to discretize the governing equations of flow and heat transfer. It is found that the aspect ratio and the porosity of the blocks influence the flow structure in the cavity. The Nusselt number of each block in the cavity improves significantly with increasing porosity; however, the influence of the aspect ratio on the Nusselt number is not significant, particularly for the Block 1.

Keywords: Flow; Porous; Heat transfer; Cavity

1. Introduction

Flow over a porous structure offers considerable advantages in the cooling applications. In a flow system, pressure drop increases with the existence of the porous structure; however, the porous structure enhances the heat transfer rates from the system. In most of the cooling applications, the heat transfer rate is a key concern rather than the pressure drop in the system. Moreover, in general, porous structure is located in channels or cavities in the cooling applications. Depending on the flow situations, the geometric orientation and the properties of the porous structure, the heat transfer rates from the heat generating body changes. Consequently, investigation into the effect of the porous blocks, their sizes, and orientations on the heat transfer rates in the cavities becomes essential.

Considerable research studies were carried out to examine flow over porous blocks. Jeng and Tzeng [1] presented a semi-empirical model for estimating the permeability and inertial coefficient of pin-fin heat sinks, which were used as porous media. They indicated that the correlations obtained from the model gave comparable results with the other tasks and concluded that for the range of Reynolds numbers ($Re = 676$–$11{,}252$), the effect of the relative fin height on the pressure drop was insignificant. Analytical and experimental studies for determining the properties of metallic foams were carried out by Bhattacharya and Mahajan [2]. They showed that thermal conductivity of the foams depended on the porosity and the ratio of the cross-sections of the fiber and the intersection. Investigation of forced convection in high porosity metal foams was carried out by Calmidi and Mahajan [3]. The empirical constants for the equations used in the numerical simulations were determined by matching the numerical predictions with the experimental data. A new model was introduced by Yu et al. [4] to account for the effects of the porosity and the pore diameter on the hydrodynamic and the thermal performance of the carbon-foam finned tube heat exchangers. They indicated that the model developed could be used to assess quantitatively the suitability of the porous carbon foam as a fin material in the design of the air–water heat exchangers. Parvazinia and Nassehi [5] modeled the flow of power law fluid in highly permeably porous medium. They indicated that a channeling occurred in the flow regime within the thin near wall boundary layer. Hassanien et al. [6] studied the unsteady flow and the heat transfer in a stagnation region of a body embedded in a porous medium. They obtained a semi-similar solution from the boundary layer equations with the use of the appropriate transformations. Naidu et al. [7] investigated the carbon foams for heating applications. They indicated that the overall heat transfer coefficients of the carbon foam heat sinks were up to two orders of magnitude

* Corresponding author. Tel.: +966 3 860 4481; fax: +966 3 860 2949.
E-mail address: bsyilbas@kfupm.edu.sa (B.S. Yilbas).

1385-8947/$ – see front matter © 2007 Elsevier B.V. All rights reserved.
doi:10.1016/j.cej.2007.07.087

Nomenclature

C_1	inertial resistance factor
E_f	fluid energy (J/kg)
E_s	solid medium energy (J/kg)
f	inertia coefficient
F	body force (N)
Gr	Grashoff number
k_{eff}	effective thermal conductivity (W/mK)
k_f	thermal conductivity of fluid (W/mK)
k_s	thermal conductivity of solid (W/mK)
K	permeability of porous block
L	width of channel (m)
n	any spatial coordinate
Nu	Nusselt number
P	pressure (Pa)
ΔP	pressure drop across the block (Pa)
$\dot{q}$	rate of heat flux (W/m^3)
S_f^h	fluid enthalpy source term (W/m^3)
T	temperature (K)
u	velocity in x-axis (m)
U_i	mean velocity at block inlet (m/s)
v	velocity in y-axis (m)
V	velocity vector
x	distance in x-axis (m)
y	distance in y-axis (m)

Greek letters

α	mass diffusivity (m^2/s)
β	thermal expansion coefficient (1/K)
ε	porosity
μ	viscosity (N s/m^3)
ν	kinematic viscosity (m^2/s)
ρ	density (kg/m^3)
τ	shear stress (N/m^2)
$\forall$	volume of the block (m^3)
$\forall_T$	total or bulk volume of material (m^3)
$\forall_v$	volume of void-space (such as fluids) (m^3)

Subscripts

eff	effective
f	fluid
i	cavity inlet
s	solid

greater than those of the conventional heat sinks. Metal foam heat sinks for the cooling application were investigated by Hetsroni et al. [8]. They indicated that the metal foam heat sink provided the superior heat transfer performance than the conventional heat exchanging devices; in which case, the Colburn factor improved significantly. The thermal characteristics of an aluminum foam heat sink were examined by Kim et al. [9]. In the analysis, they assumed that the solid was in the local thermal equilibrium with the fluid. They indicated that the anisotropy in the permeability and the effective thermal conductivity yield a significant change in the heat transfer rates. The mass and heat transport in the ceramic foams were examined by Richardson et al. [10]. They showed that the ceramic foams reduced the pressure drop by a factor of about 10 and the flow through the foam structure followed the same convective behavior to that observed in the packed beds. The characteristics of oscillating flow through a channel filled with a metal foam structure were investigated by Leong and Jin [11]. They indicated that the pressure drop and the velocity profiles of the oscillating flow in the open-cell metal foam increased with the increase of the Reynolds number and the dimensionless flow amplitude.

In the present study, the flow over two porous blocks in the cavity is considered and the heat transfer rates from the porous blocks are numerically computed. In the simulations, three porosities and three aspect ratios are accommodated to examine the effects of the porosity and aspect ratio on the heat transfer rates. The Reynolds number at cavity inlet is kept at 100 and a constant heat flux source is employed in the porous blocks, provided that the simulations are repeated for the Reynolds number of 200 at the cavity inlet for the comparison.

2. Mathematical analysis

The equations governing the flow over porous blocks situated in a cavity can be formulated through considering the equilibrium equations. In this case, porous medium can be defined as a material consisting of a solid matrix with an interconnected void, provided that a single fluid (single phase) occupies the voids spaces. After assuming an isotopic porosity and a single phase steady flow, the volume-averaged mass and momentum conservation equations for a steady flow situation can be written in vector notation as:

$$\nabla \cdot (\varepsilon \rho V) = 0 \tag{1}$$

and

$$\nabla \cdot (\varepsilon \rho V V) = -\varepsilon \nabla p + \nabla \cdot (\varepsilon \tau) + \varepsilon F - \left(\frac{\mu}{\alpha} + \frac{C_1 \rho}{2} |V| \right) V \tag{2}$$

The last term in this equation represents the viscous (Darcy loss term) and inertial drag forces imposed by the pore walls on the fluid. Note that ε is the porosity of the media defined as the ratio of the volume occupied by the fluid to the total volume. However, the term $((\mu/\alpha) + (C_1\rho/2)|V|)V$ in Eq. (2) is the source term due to the porous media. However, outside of the porous media, the source term drops and $\varepsilon = 1$. Therefore, Eq. (2) reduces to the standard momentum equation for a single phase steady fluid flow.

The coefficient α in the viscous loss term equals to K, permeability of the porous structure. The coefficient C_1 in the inertial loss term is written as:

$$C_1 = \frac{f}{\sqrt{K}}$$

f is the inertia coefficient reflecting porous inertia effects. However, K and f are related to structure of the porous medium as given by Bhattacharya et al. [12]. The values of K and f are given in Table 1 for two porous blocks.

Table 1
Properties of porous blocks used in the simulations

Porosity (ε)	f	K ($\times 10^7$ m^2)
0.9726	0.097	2.7
0.8991	0.068	0.94

The standard energy transport equation in porous media regions is solved with modifications to the conduction flux and the transient terms only. In the porous medium, the conduction flux uses an effective conductivity and the transient terms includes the thermal inertia of the solid region on the medium

$$\nabla \cdot (V(\rho_f E_f + P)) = \nabla \cdot (k_{eff} \nabla T - \tau \cdot V) + S_f^k \quad (3)$$

where the effective thermal conductivity in the porous medium, k_{eff}, is the volume average of the fluid conductivity and the solid conductivity.

$$k_{eff} = \varepsilon k_f + (1 - \varepsilon) k_s \quad (4)$$

where E_f is the fluid energy per unit mass, k_f the fluid phase thermal conductivity (including the turbulent contribution (k_t)), k_s the solid medium thermal conductivity, k_{eff} the effective thermal conductivity of the medium, S_f^k the fluid enthalpy source term, ε the porosity of the medium, V the velocity vector, τ the shear stress, P the pressure, and F is the body force including that due to buoyancy. The porosity is defined by the ratio:

$$\varepsilon = \frac{\forall_v}{\forall_T}$$

where $\forall_v$ is the volume of void-space (such as fluids) and $\forall_T$ is the total or bulk volume of material, including the solid and void components.

In the case of fluid side, the governing equations of flow are modified, and ε in Eqs. (1)–(3) is set to 1. In addition, k_{eff} is becomes k_f (fluid thermal conductivity) in Eq. (4).

The Nusselt number is determined from:

$$Nu = \frac{\overline{hL}}{k_{eff}}$$

where L is the wetted perimeter of the heated section of the porous media. The Grashoff number is defined by:

$$Gr = \frac{g\beta(T_s - T_i)L^3}{\nu^2}$$

where T_s is the average surface temperature of the porous media and L is the length of the porous block.

2.1. Boundary conditions

Two solid blocks with different geometric arrangements in the cavity is considered. The rectangular blocks are accommodated while the surface area of each block is kept the same. Fig. 1 shows the schematic view of the solution domain (cavity and the geometric configurations of the blocks) while Table 2 gives the geometric dimensions of the solution domain. The blocks are numbered in such away that the first block is defined as Block 1 and the second block is named as Block 2 in the cavity. The

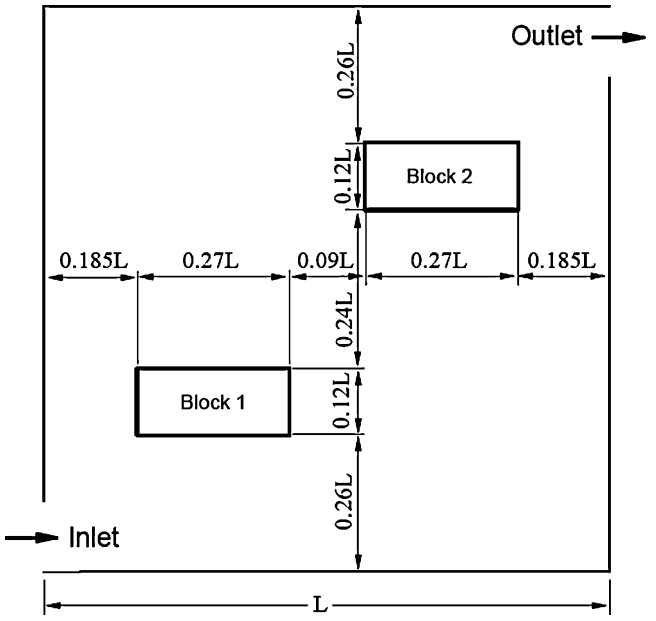

Fig. 1. Dimensions of cavity and configurations of the blocks. $L = 0.05$ m and the aspect ratio = 2.25.

geometric arrangement of blocks in the cavity is named as configurations; therefore, four configurations of blocks in the cavity are employed in the simulations. The selection of the cavity and block sizes are based on the flow conditions resulting in equally importance of the natural and the forced convection currents in the cavity for a mixed flow like situation. Moreover, the velocity magnitude is normalized through diving it by the cavity inlet velocity.

The adiabatic cavity walls with no slip and impermeable wall conditions for the velocity components are considered, i.e.

$$\frac{\partial T}{\partial n} = 0, \quad u = v = 0$$

The pressure boundary is assumed at cavity exit while the uniform flow and temperature are assumed at cavity inlet, i.e.

$$\frac{\partial \varphi}{\partial n} = 0$$

where φ is any property of the fluid.

The uniform heat flux ($q = 4 \times 10^5$ W/m^3) is introduced in the rectangular porous and solid blocks (reference to Fig. 1). The temperature and heat flux continuity are assumed at solid

Table 2
Block and cavity dimensions, aspect ratios and porosities used in the simulations

Cavity length	L (0.05 m)
Cavity width	L (0.05 m)
Total area of each block	$(0.18L)^2$ (8.1×10^{-5} m^2)
Cavity inlet port size	$0.2L$ (0.01 m)
Cavity exit port size	$0.2L$ (0.01 m)
Cavity inlet velocity	0.1544 m/s
Re_{inlet}	100
Rate of heat flux	5×10^5 W/m^3
Porosity for each block	0.9726 and 0.8991
Aspect ratios of block	1/2.25; 1; 2.25

Table 3
Properties of the fluid and solid block used in the simulations

	Air	Solid block
Density (kg/m^3)	1.177	7836
Specific heat (J/kg K)	1005	969
Thermal conductivity (W/m K)	0.02565	28.2
Viscosity (m^2/s)	1.544×10^{-5}	–

block–fluid interface, i.e.

$$T_s = T_f \quad \text{and} \quad k_s\left(\frac{dT}{dn}\right)_s = k_f\left(\frac{dT}{dn}\right)_f$$

Air is used as the flowing fluid while solid block is considered to be steel. The properties of air at standard pressure and temperature and thermal properties of block are given in Table 3.

2.2. Numerical solution

The control volume approach is employed in the numerical scheme. All the variables are computed at each grid point except the velocities, which are determined midway between the grid points. The details of control volume approach are given by Patankar [13]. The grid independent tests are carried out and 192 × 192 grid size are selected on the basis of grid independent solutions with less computation time.

A staggered grid arrangement is used in he present study, which provides the pressure linkages through the continuity equation and is known as SIMPLE algorithm as presented by Patankar [13]. This procedure is an iterative process for convergence. The pressure link between continuity and momentum is established by transforming the continuity equation into a Poisson equation for pressure.

3. Model validation

To validate the numerical model, an experimental work carried out previously [3] for the metal foam is simulated. The simulation conditions are kept identical to the experimental set up and the test parameters. In this case, a fully developed flow inlet to the duct partially filled with the metal foam with 63 mm × 45 mm × 114 mm size is considered. Air is used as the working fluid. The constant heat generation from the top and bottom walls of the duct is accommodated. The characteristics of the metal foam are given in Table 4. In the simulations the grid independent tests are carried out to ensure the grid independent solution. Fig. 2 shows the comparison of the model predictions and the experimental for the wall temperature above ambient with the axial distance. It can be observed that both results are in good agreement.

Table 4
Metal foam characteristics used in the simulations

Porosity (ε)	0.9118
f	0.085
K ($\times 10^7$ m^2)	1.8

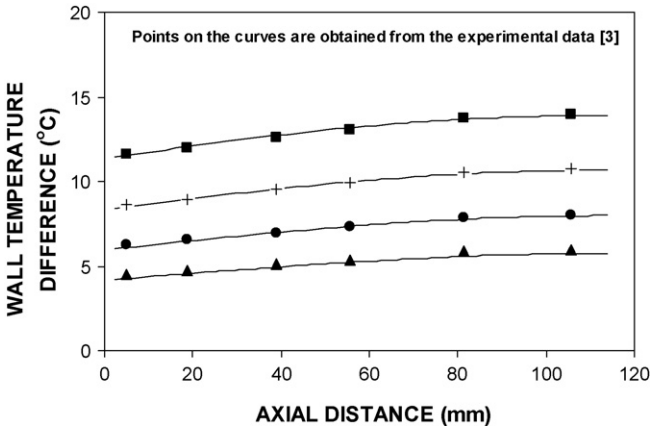

Fig. 2. Wall temperature difference predicted and obtained from the experimental data along the axial distance. The curves represent the predictions for different inlet average velocities while the dotted points are obtained from the experimental data [3] for different inlet averaged velocities.

4. Results and discussion

Flow over porous blocks in the cavity is examined for three aspect ratios and three porosities of the blocks. The heat transfer rates from each block are computed and findings are discussed accordingly. Air is used as the working fluid and Table 3 gives the properties of the fluid used in the simulations.

Fig. 3(a) shows normalized velocity (V/V_i) contours in the cavity for three aspect ratios and porosities while Fig. 3(b) shows the velocity vectors in the cavity. It should be noted that the porosity $\varepsilon = 0$ represents the solid block, which is included for the comparison. Flow entering the cavity partially spills around the Block 1 (Fig. 1) and it merges in the exit region of the cavity for the aspect ratio of 1:2.25. As the aspect ratio increases, the flow field in the cavity modifies and the flow spilling occurs in the upstream of the Block 2 (Fig. 1) and it merges in the downstream of the block. Moreover, the blockage affect of the Block 1 in the cavity is responsible for the flow splitting around the Block 2. In this case, the fluid mainly passes below the Block 1 and, then, spills around the Block 2. However, the natural convection current generated above the Block 1 does not significantly contribute to the flow mixing in the cavity. Consequently, the low velocity flow is generated above the Block 1. This situation is particularly true for the aspect ratios $\alpha \geq 1$. As the porosity increases, the flow penetration through and emerging from the block contributes to the enhancement of the forced convection current in the downstream of the blocks. Moreover, the flow acceleration and attainment of the high velocity in the region below the Block 1 is suppressed by the increasing porosity. It should be noted that the flow acceleration below the Block 1 is because of the blockage affect of the Block 1 at the cavity inlet, i.e. throttling of the flow between the bock and the cavity wall results in the flow acceleration in this region. The flow merging at the cavity inlet results in high flow velocity in this region. This situation is true for all the aspect ratios and porosities.

Fig. 4 shows normalized temperature (T/T_i) contours in the cavity for three aspect ratios and porosities. In the case of solid

block ($\varepsilon = 0$), the thermal boundary layer developed around the blocks enhances the high temperature region around the blocks, particularly when the forced convection current is small. Consequently, the natural convection current contributes to the extension of the high temperature region in the cavity. Moreover, temperature remains low in the region when the forced convection current is high, i.e. in the region of cavity bottom. As the porosity increases, the flow penetrating through the blocks mixes with the natural convection current, which in turn lower temperature in the natural convection current. This is particularly true for the Block 1 and porosity $\varepsilon = 0.972$. Moreover, thinning of the thermal boundary layer around the surfaces of the porous blocks also contributes to the attainment of the low temperature field in the downstream of the porous Block 1. The locally extension of the temperature field in the cavity indicates that the cooling rates for each block is dependent on the aspect ratio and porosity. However, the effect of porosity on the cooling rates is more pronounced than that of the aspect ratio. This is because of the flow penetrating through the porous block significantly influences the temperature fields in the downstream of the block, which is more pronounced for the Block 1.

Fig. 5 shows the Nusselt number variation with the aspect ratio for two blocks and three porosities. It should be noted that Block 1 and Block 2 in the cavity are shown Fig. 1 and the simulations are repeated for six different aspect ratios to produce Fig. 5. In order to accommodate the effect of the cavity inlet Reynolds number on the heat transfer rates, the Nusselt number obtained for $Re = 200$ is also given in Fig. 5. The effect of aspect ratio on the Nusselt number is almost insignificant for the solid Block 1. However, the influence of porosity on the Nusselt number is significant in such away that increasing porosity significantly enhances the heat transfer rates from the Block 1. This is because of the low temperature flow emerging from the cavity inlet and penetrating through the porous Block 1, i.e. it enhances the convection rates. As the porosity decreases, the cooling rates of the Block 1 reduces and the influence of the forced convection current on the heat transfer rates replaces with the cooling due to natural convection current. In the case of the Block 2, the Nusselt number increases with increasing the aspect ratio for the aspect ratios $\alpha \leq 1.5$, and further increases in the aspect ratio results in monotonic behavior of the Nusselt number. The flow spilling around the Block 2 improves the heat transfer rates,

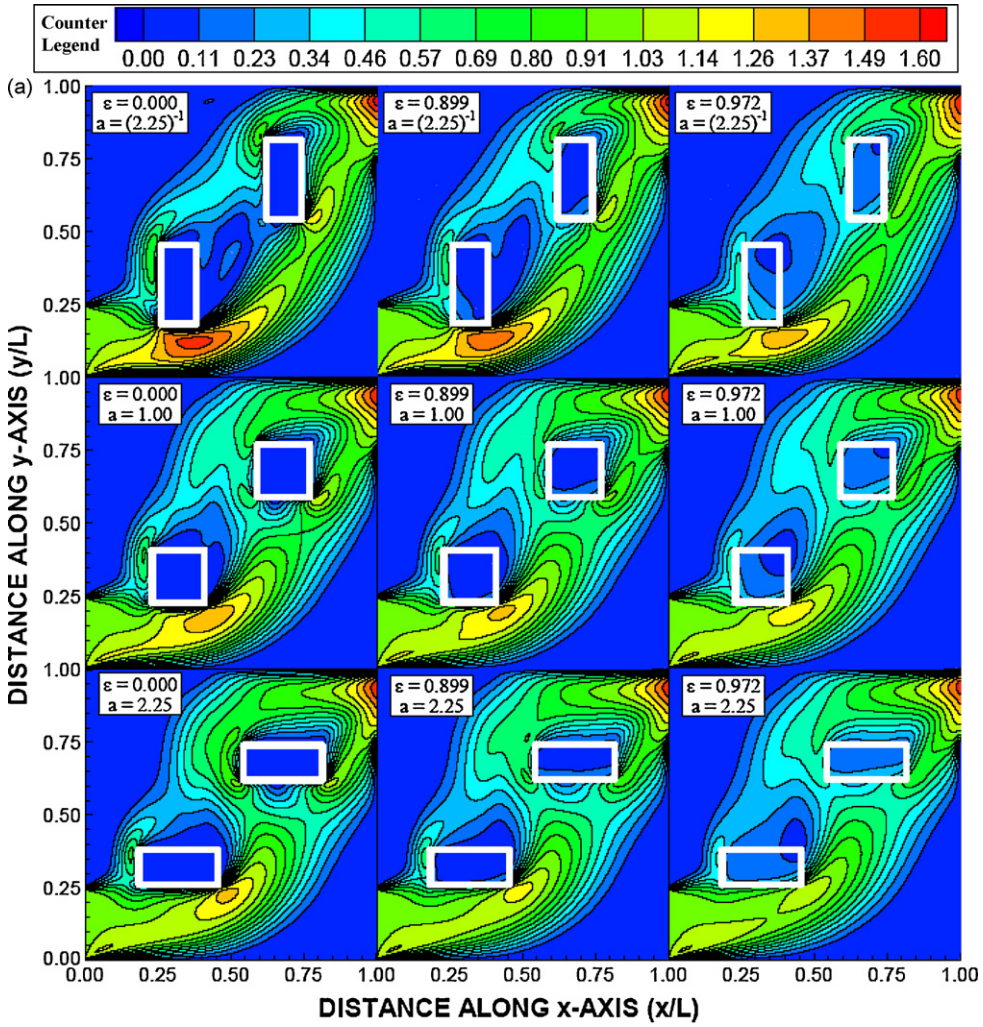

Fig. 3. (a) Normalized velocity magnitude (V/V_i) for different aspect ratios and the porosities. (b) Velocity vectors in the cavity for different aspect ratios and the porosities.

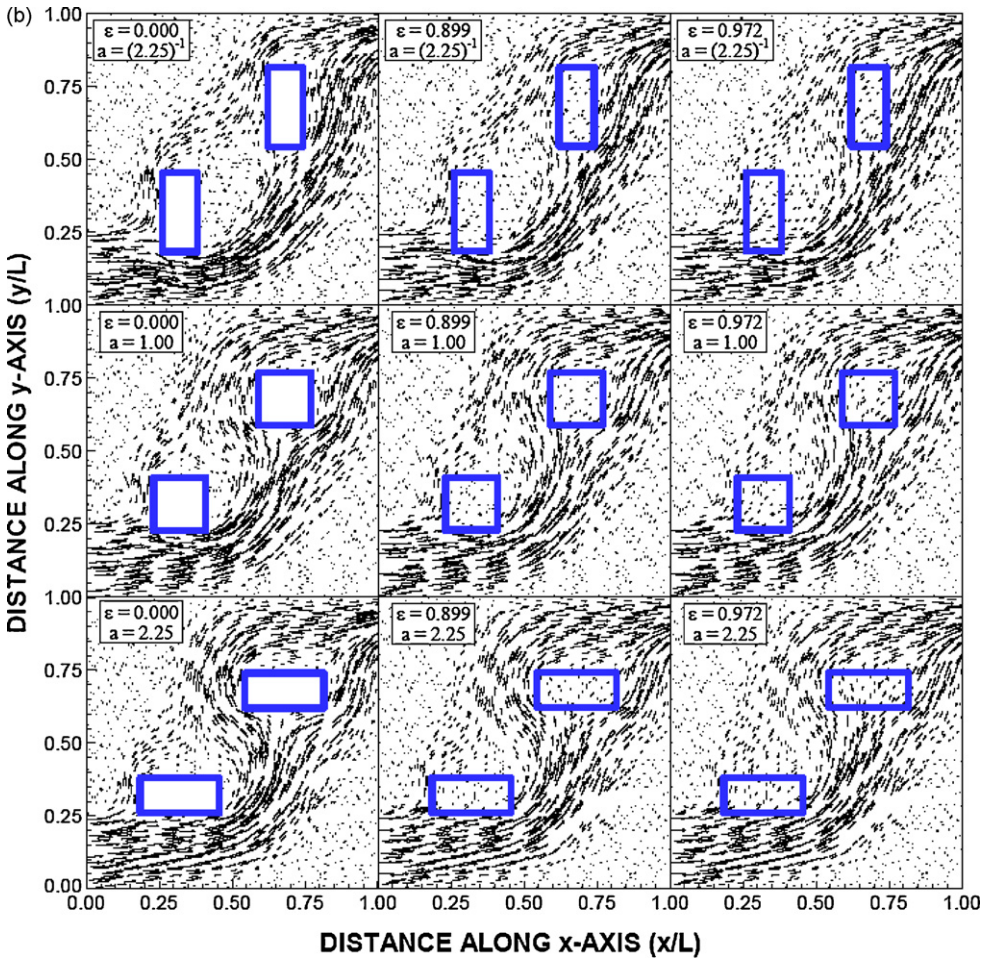

Fig. 3. (*Continued*).

particularly for the aspect ratios $\alpha \geq 1.5$. In the case of the solid block, enhancement of heat transfer rates is associated with the thinning of the thermal boundary layer due to forced convection. Increasing porosity enhances the heat transfer rates from the porous blocks because of the flow penetrating through the porous structure. However, mixing of the natural and forced convection currents in the downstream of the Block 2 generates the high temperature region extending towards the cavity exit. This suppresses the heat transfer rates. This situation is more pronounced for the aspect ratios $\alpha \leq 1.5$. However, flow penetrating the porous block reduces the size of the thermal boundary layer, particularly above the Block 2. This in turn lowers the fluid temperature in the upper region and downstream of the block. Consequently, the heat transfer rates improve. This situation is more pronounced for the aspect ratios $\alpha \geq 1.5$. When comparing the Nusselt number for both blocks, it can be observed that the Nusselt number corresponding to the Block 1 is higher than that of the Block 2. This is true for all the aspect ratios and the porosities. This is because of the location of the Block 1, which is closer to the cavity inlet where the low temperature fluid enters the cavity. The effect of the Reynolds number on the Nusselt number is more pronounced for the Block 1; in which case, the Nusselt number increases significantly for all porosities employed in the simulations. However, in the case of the Block 2, the improvement in the Nusselt number is not notable including the solid block ($\varepsilon = 0$).

Fig. 6 shows the variation of the Grashoff number with the aspect ratios and three porosities. It should be noted that in order to accommodate the effect of the cavity inlet Reynolds number on the heat transfer rates, the Grashoff number obtained for $Re = 200$ is also given in Fig. 6. In the case of the Block 1, the Grashoff number attains high values for the solid block and it reduces with increasing porosities. The attainment of high Grashoff number for the solid block indicates that the natural convection current is important for the heat transfer rates from the blocks. However, the slight change of the Grashoff number with the aspect ratio shows that the thinning of the thermal boundary layer around the block due to forced convection current does not have significant effect on the natural convection current. Increasing porosity improves the flow penetration through the block while lowering the thermal boundary layer thickness around the block. In addition, mixing of the forced and the natural convection currents lowers the fluid temperature emanating from the block. Consequently, the Grashoff number reduces significantly with the increasing porosity, provided that the effect of aspect ratio on the Grashoff number is not considerable. In the case of the Block 2, the Grashoff number reduces with the increasing aspect ratio. This is true for all the porosi-

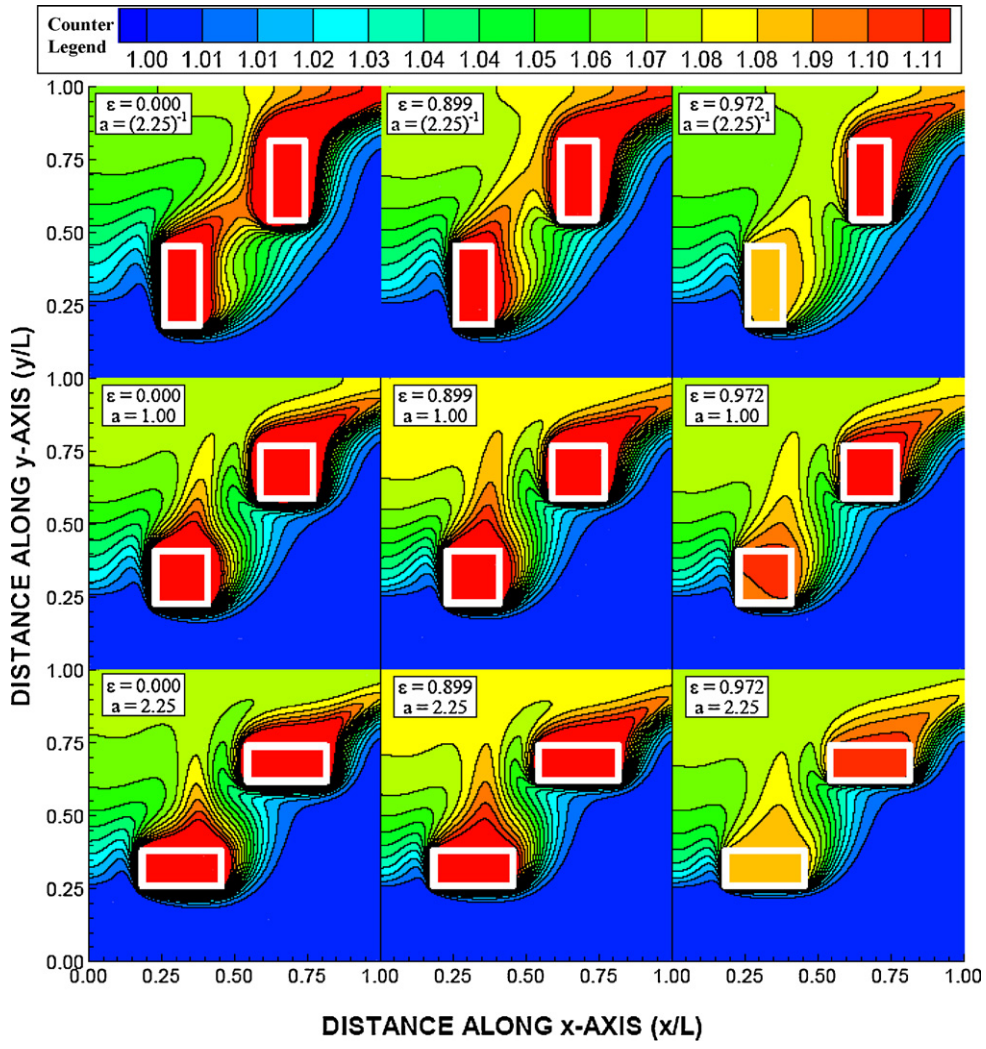

Fig. 4. Normalized temperature (T/T_i) for different aspect ratios and the porosities.

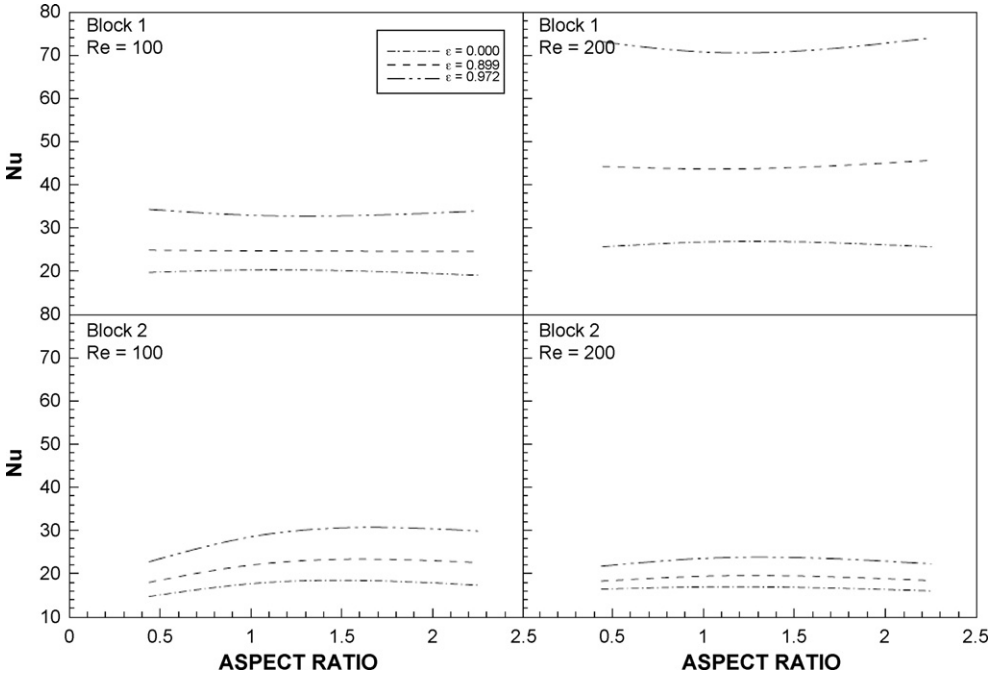

Fig. 5. Nusselt number variation with the aspect ratio for two blocks and different porosities.

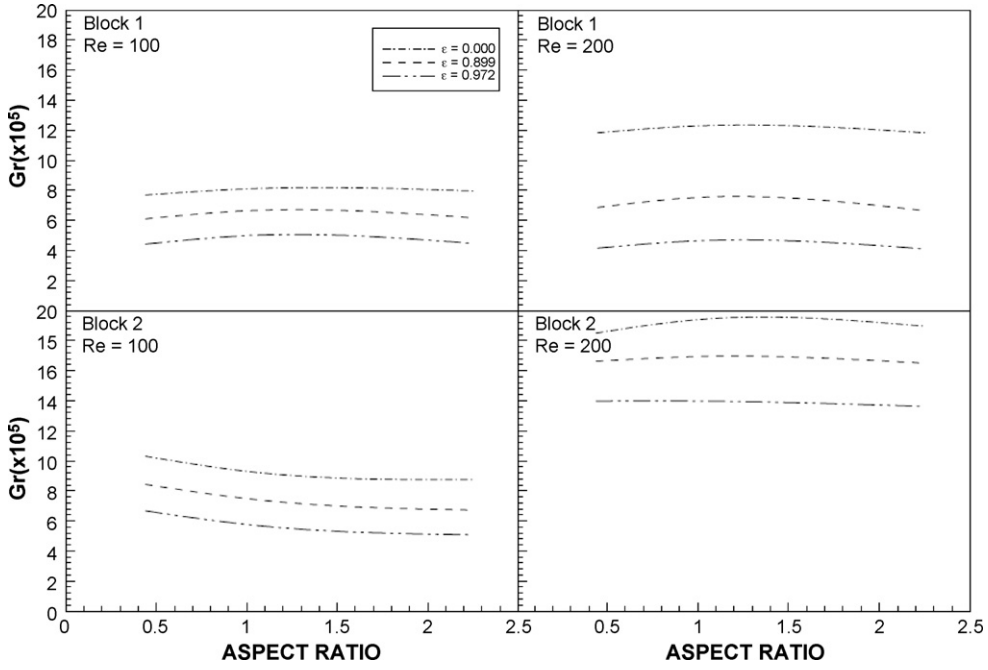

Fig. 6. Nusselt number variation with the aspect ratio for two blocks and different porosities.

ties. Decreasing of the Grashoff number with the aspect ratio is associated with the thickness of the thermal boundary layer thickness and the natural convection current developed around the Block 2. Due to the high temperature fluid in the downstream of the Block 1 suppresses the forced convection cooling of the blocks, which in turn thickens the thermal boundary layer thickness around the block. When comparing the Grashoff number of both blocks, it is evident that Block 2 results in higher Grashoff number than that of the Block 1. This difference is marginal for the solid block and it is significant for the porous blocks. The effect of the Reynolds number on the Grashoff number is more pronounced for the Block 2; in which case, the Grashoff number increases significantly for all porosities employed in the simulations. However, in the case of the Block 1, the improvement in the Nusselt number is notable for the solid block ($\varepsilon = 0$).

5. Conclusion

Thermal analysis of the porous blocks situated in the cavity is examined and the flow field and heat transfer rates from the blocks are computed numerically. The simulations include three aspect ratios and three porosities of the blocks. Air is used as the working fluid and the Reynolds number is kept constant at the cavity inlet ($Re = 100$). It is found that the flow structure changes with the aspect ratio and porosities. The partial splitting of the flow in the upstream of the Block 1 is observed for the aspect ratio $\alpha = 1{:}2.25$ while the flow splitting in the upstream of the Block 2 occurs for the aspect ratios $\alpha \geq 1$. The flow acceleration at the bottom of the Block 1 is observed due to the blockage effect of the Block 1 in the cavity inlet region. The contribution of the natural convection current and the flow penetration of the porous blocks results in the extension of the high temperature region above the blocks. The Nusselt number variation with the aspect ratio is not considerable for the Block 1. However, the effect of porosity on the Nusselt number is significant. In this case, increasing the porosity enhances the Nusselt number. This is attributed to the cooling enhancement of the blocks through the flow penetration of the porous blocks. In the case of the Block 2, the Nusselt number increases with increasing the aspect ratio. This is associated with the location of the Block 2; in which case, the fluid heated in the downstream of the Block 1 suppresses the heat transfer rates from the Block 2. The Grashoff number remains almost the same for all the aspect ratios; however, it reduces significantly with increasing porosity. This is true for both blocks. In the case of the Block 2, the Grashoff number decreases with increasing aspect ratio.

Acknowledgements

Acknowledgements are due to King Fahd University of Petroleum and Minerals.

References

[1] T.M. Jeng, S.C. Tzeng, Numerical study of confined slot jet impinging on porous metallic foam heat sink, Int. J. Heat Mass Transfer 48 (2005) 4685–4694.
[2] Bhattacharya, R.L. Mahajan, Finned metal foam heat sinks for electronics cooling in forced convection, J. Electron. Pack. 124 (2002) 155–163.
[3] V.V. Calmidi, R.L. Mahajan, Forced convection in high porosity metal foams, ASME J. Heat Transfer 122 (2000) 557–565.
[4] Q. Yu, A.G. Straatman, B.E. Thompson, Carbon-foam finned tubes in air–water heat exchangers, Appl. Therm. Eng. 26 (2006) 131–143.
[5] M. Parvazinia, V. Nassehi, Study of shear thinning fluid flow through highly permeable porous media, Int. Commun. Heat Mass Transfer 33 (4) (2006) 401–410.
[6] I.A. Hassanien, F.S. Ibrahim, G.M. Omer, Unsteady flow and heat transfer of a viscous fluid in the stagnation region of a three-dimensional body embedded in a porous medium, J. Porous Media 9 (4) (2006) 357–372.

[7] S.V. Naidu, V.D. Rao, P.K. Sarma, T. Subrahmanyam, Performance of a circular fin in a cylindrical porous enclosure, Int. Commun. Heat Mass Transfer 31 (2004) 1209–1218.
[8] G. Hetsroni, M. Gurevich, R. Rozenblit, Sintered porous medium heat sink for cooling of high-power mini-devices, Int. J. Heat Fluid Flow 27 (2006) 259–266.
[9] S.Y. Kim, J.W. Paek, B.H. Kang, Flow and heat transfer correlations for porous fin in a plate-fin heat exchanger, ASME J. Heat Transfer 122 (2000) 572–578.
[10] J.T. Richardson, D. Remue, J.K. Hung, Properties of ceramic foam catalyst supports: mass and heat transfer, Appl. Catal. A: Gen. 250 (2003) 319–329.
[11] K.C. Leong, L.W. Jin, Characteristics of oscillating flow through a channel filled with open-cell metal foam, Int. J. Heat Fluid Flow 27 (2006) 144–153.
[12] A. Bhattacharya, V.V. Calmidi, R.L. Mahajan, Thermophysical properties of high porosity metal foams, Int. J. Heat Mass Transfer 45 (2002) 1017–1031.
[13] S.V. Patankar, Numerical Heat Transfer and Fluid Flow, Hemisphere Publishing Company, Washington, DC, 1980.